Transport cross sections and collision integrals for C⁺(^{2}P)–H(^{2}S), C(^{3}P)–H⁺(^{1}S), C(^{1}D)–H⁺(^{1}S), and C⁺(^{4}P)–H(^{2}S) interactions ⊘

Zhenlu Hou (后振鲁) ⓘ ; Zhi Qin (秦智) ✉ ⓘ ; Linhua Liu (刘林华) ⓘ

CrossMark

🌐 View Online

📄 Export Citation

Articles You May Be Interested In

Microring bio-chemical sensor with integrated low dark current Ge photodetector

Appl. Phys. Lett. (March 2015)

On the uncertainty of the Auger recombination coefficient extracted from InGaN/GaN light-emitting diode efficiency droop measurements

Appl. Phys. Lett. (March 2015)

Energy gap induced by the surface optical polaron in graphene on polar substrates

Appl. Phys. Lett. (March 2015)

Transport cross sections and collision integrals for C$^+$(^{2}P)–H(^{2}S), C(^{3}P)–H$^+$(^{1}S), C(^{1}D)–H$^+$(^{1}S), and C$^+$(^{4}P)–H(^{2}S) interactions

Zhenlu Hou (后振鲁),[1,2] (iD) Zhi Qin (秦智),[1,2,a] (iD) and Linhua Liu (刘林华)[1,2,3,b] (iD)

AFFILIATIONS

[1]School of Energy and Power Engineering, Shandong University, Jinan 250061, People's Republic of China
[2]Optics and Thermal Radiation Research Center, Institute of Frontier and Interdisciplinary Science, Shandong University, Qingdao 266237, People's Republic of China
[3]School of Energy Science and Engineering, Harbin Institute of Technology, Harbin 150001, People's Republic of China

[a]Author to whom correspondence should be addressed: z.qin@sdu.edu.cn
[b]Electronic mail: liulinhua@sdu.edu.cn

ABSTRACT

Transport collision integrals of interacting atoms or ions play a crucial role in modeling transport properties of high-temperature gases and plasmas. Here, we obtained the potential energy curves (PECs) of CH$^+$ using the internally contracted multireference configuration interaction method with the Davidson correction (icMRCI+Q) method. The PECs were then used to investigate the transport cross sections and transport collision integrals for the C$^+$(^{2}P)–H(^{2}S), C(^{3}P)–H$^+$(^{1}S), C(^{1}D)–H$^+$(^{1}S), and C$^+$(^{4}P)–H(^{2}S) interactions using the classical mechanical approach and a quantum mechanical treatment of the scattering with Wentzel–Kramers–Brillouin approximations of the scattering phase shifts. The transport cross sections were obtained in the collision energy of 10^{-6}–1 hartree, which were used to compute transport collision integrals for C–H$^+$ and C$^+$–H systems over the temperature range of 500–40 000 K. The C(^{1}D)–H$^+$(^{1}S) and C$^+$(^{4}P)–H(^{2}S) interactions are considered for the first time. Our transport collision integrals can provide data references for computing transport properties of high-temperature plasmas involving C and H atoms/ions.

Published under an exclusive license by AIP Publishing. https://doi.org/10.1063/5.0171776

I. INTRODUCTION

The methylidyne cation, CH$^+$, has been detected in a variety of astronomical environments, including the Orion Bar photodissociation region (PDR),[1] interstellar medium (ISM),[2] envelope of the Red Rectangle,[3] planetary nebula NGC 7027,[4] the massive star-forming region DR21,[5] Herbig Be star HD 100546,[6] distant high-mass star-forming regions (SFRs),[7] diffuse molecular clouds,[8,9] and Titan atmosphere.[10] CH$^+$ is quite abundant in the interstellar space, which is believed to be one of the most important building blocks of interstellar organic molecules[11] and to be of great significance in astrophysics.[7,12–14] CH$^+$ has also attracted great attention in the industry. For example, the CH$^+$ plasma is closely linked to the critical fusion reactor design issue of tritium codeposition in tokamaks with carbon as wall material.[15] Modeling the astronomical environments containing C and H atoms/ions or the related plasmas usually requires their transport coefficients, including the viscosity, thermal conductivity, electrical conductivity, and so on.

Transport coefficients at high temperatures are very difficult to measure in experiments; thus, theoretical calculations are widely used.[16] For the heteronuclear neutral-ion interactions (e.g., X$^+$–Y and X–Y$^+$ interactions), the transport coefficients can be determined using the transport collision integrals, which can be obtained based on the transport cross sections,[17–20] such as the momentum-transfer cross section (MTCS) and viscosity cross section (VCS). The charge exchange cross sections for collisions between heteronuclear neutrals and ions are small compared to the elastic transport collision integrals (including MTCS and VCS) and can be neglected.[21] To obtain the first order approximation of diffusion coefficient and viscosity coefficient, the MTCS and the VCS are required, respectively. For the second or third order approximation of transport coefficients, such as electrical conductivity and thermal conductivities, the third moment cross section $Q^{(3)}$ is required.

As early as 2002, Schultz and Krstić[22] reported transport cross sections for the C(^{3}P)–H$^+$(^{1}S) interaction using one-channel quantum

mechanical (QM) method based on *ab initio* PECs in the energy range of 0.1–200 eV. Sourd *et al.*[23] determined transport cross sections and transport collision integrals for the interactions of 12 atoms and atomic ions in e/C/H/N/O mixtures, which were used to obtain their transport coefficients in the temperature range of 9000–20 000 K at $p = 1$ bar and 11 000–20 000 K at $p = 10$ bar, in which $C^+(^2P)$–$H(^2S)$ and $C(^3P)$–$H^+(^1S)$ interactions were considered. Transport cross sections for the $C^+(^2P)$–$H(^2S)$ and $C(^3P)$–$H^+(^1S)$ interactions were investigated by Liu *et al.*[24] using the multichannel quantal molecular orbital close-coupling (QMOCC) method based on *ab initio* PECs in the energy range of 10^{-4}–10 eV. Sanon and Baronnet[25] calculated the transport coefficients for the thermal plasma composed of Ar/C/H/O/N in the temperature range from 1000 to 15 000 K based on the transport collision integrals for 595 interactions, including $C^+(^2P)$–$H(^2S)$ and $C(^3P)$–$H^+(^1S)$ interactions. Subsequently, a systematic study of high-temperature transport coefficients of the carbon and water mixtures was undertaken by Wang *et al.*,[26] who computed the transport coefficients for the $C(^3P)$–$H^+(^1S)$ interaction using the transport collision integrals from Sourd *et al.*[23] The investigations mentioned above only focused on the $C^+(^2P)$–$H(^2S)$ and $C(^3P)$–$H^+(^1S)$ interactions and did not present the specific values of transport collision integrals. Other possible interactions between the atomic ground and excited states in the related plasmas, such as $C(^1D)$–$H^+(^1S)$ and $C^+(^4P)$–$H(^2S)$ interactions, are also of paramount importance at high temperatures because the high-temperature environment can trigger off the formation of excited-state neutrals and ions, whose numbers increase with increasing temperature.[27]

The quantum approach and the classical mechanical (CM) approach are used frequently to calculate the transport cross sections. Recently, Buchowiecki and Szabó[28] computed the transport cross sections and transport collision integrals of the N–H, N–H+, H–N+, and O–O systems using the CM approach and a quantum mechanical treatment of the scattering with Wentzel–Kramers–Brillouin (WKB) approximations of the scattering phase shifts (named QM-WKB in this work), considering the temperature range of 300–1000 K. For the considered most temperatures, the discrepancies between the collision integrals obtained by both methods are less than 1% and the collision integrals for the repulsive potentials computed by the CM and QM-WKB methods show good agreement. Note that the accuracy of transport cross sections and transport collision integrals is not only influenced by the theoretical and computational methods but also strongly relies on the reliability of the underlying potential energy curves (PECs).

The analytical potential energy functions used frequently to calculate the transport collision integrals, including Lennard-Jones (LJ),[29–34] m-6-8,[35,36] Hulburt–Hirschfelder (HH),[35,37,38] Murrell–Sorbie (MS),[39] and modified morse (MM)[40] potentials, rely on the experimental spectroscopic data and can produce accurate potential wells of PECs. However, it is questionable in the resulting transport collision integrals due to the uncertainty of PECs in both the dissociated asymptotic and short-range regions. In addition, the excited states, particularly repulsive ones, are believed to have a significant impact on determining the transport collision integrals.[27] Buchowiecki and Szabó[41] concluded that using a simple exponential function to represent the repulsive PECs is not suitable for accurately calculating transport collision integrals across a wide range of temperatures. They also compared the transport collision integrals computed

using the CM method based on various PECs, such as HH, MS, and *ab initio* PECs, and pointed out that high-quality *ab initio* potential energy points are needed to obtain reliable transport collision integrals. To mitigate the issues stated above, it is essential to adopt accurate PECs across the whole internuclear distance, which can be used to obtain reliable transport collision integrals and then effectively predict transport properties.

With the development of quantum chemistry methods,[42–45] the computational accuracy of *ab initio* PECs has improved significantly. *Ab initio* potential energy data can be accepted as a baseline when experimental spectroscopic data are not available. As early as 1995, Aziz *et al.*[46] obtained the transport properties and virial coefficients of helium based on the state-of-the-art *ab initio* PECs. Transport collision integrals for the $N(^4S)$–$H(^2S)$, $N(^2D)$–$H(^2S)$, and $N(^2P)$–$H(^2S)$ interactions together with the H–N+, N–H+, N2+–H, and N+–H+ interactions are calculated and analyzed by Buchowiecki and Szabó[27,41] based on *ab initio* PECs. The transport cross sections and integrated cross sections for interactions of hydrogen and nitrogen atoms and ions in their ground and excited states are also obtained by Buchowiecki[47] using the CM approach and the QM-WKB method based on extrapolated *ab initio* PECs. In our group, Ding *et al.*[48] calculated transport collision integrals for $N(^4S)$–$N(^4S)$, $N(^4S)$–$N(^2D)$, and $N(^4S)$–$N(^2P)$ interactions using the analytically fitted the combined-hyperbolic-inverse-power-representation (CHIPR)[49–57] functions to high-level *ab initio* potential energy points of N2. The CHIPR method can give nearly the same transport collision integrals as those from the interpolation and extrapolation of *ab initio* potential energy points, but this method may cost huge time on fitting PECs for all the electronic states. The collision data, including the resonant charge exchange and elastic cross sections as well as the inelastic, elastic, and total transport collision integrals, for the $N(^4S)$–$N^+(^3P)$ and $N(^4S)$–$N^+(^1D)$ interactions, were also obtained by Ding *et al.*[58] using the QM-WKB method based on *ab initio* potential energy points. Hou *et al.*[59] obtained the transport collision integrals for the $C(^3P)$–$H(^2S)$, $C(^5S)$–$H(^2S)$, $C(^1S)$–$H(^2S)$, and $C(^1D)$–$H(^2S)$ interactions based on the extrapolated *ab initio* PECs of CH over the temperature range of 500–50 000 K. Therefore, using the *ab initio* potential energy points is a significant ingredient for accurate calculations of transport collision integrals.[27,58,59]

Given the above consideration, this work aims to use QM-WKB and CM methods to calculate the transport cross sections for elastic collisions of carbon and hydrogen atoms and ions (C^+–H and C–H+) based on the state-of-the-art *ab initio* PECs and then to determine transport collision integrals for $C^+(^2P)$–$H(^2S)$, $C(^3P)$–$H^+(^1S)$, $C(^1D)$–$H^+(^1S)$, and $C^+(^4P)$–$H(^2S)$ interactions. Section II provides the theory and methods for computing PECs, transport cross sections, and

TABLE I. Statistical weights for the electronic states of CH^+.

$C^+(^2P)$–$H(^2S)$		$C(^3P)$–$H^+(^1S)$		$C(^1D)$–$H^+(^1S)$		$C^+(^4P)$–$H(^2S)$	
State	w_i	State	w_i	State	w_i	State	w_i
X $^1\Sigma^+$	1/12	1 $^3\Sigma^-$	3/9	2 $^1\Sigma^+$	1/5	2 $^3\Sigma^-$	3/24
A $^1\Pi$	2/12	2 $^3\Pi$	6/9	1 $^1\Delta$	2/5	3 $^3\Pi$	6/24
a $^3\Pi$	6/12			2 $^1\Pi$	2/5	1 $^5\Sigma^-$	5/24
1 $^3\Sigma^+$	3/12					1 $^5\Pi$	10/24

TABLE II. Electronic states of CH$^+$ and their corresponding dissociation limits.

Dissociation limit	Molecular electronic states
C$^+$(^{4}P)–H(^{2}S)	2 $^3\Sigma^-$, 3 $^3\Pi$, 1 $^5\Sigma^-$, and 1 $^5\Pi$
C(^{1}D)–H$^+$(^{1}S)	2 $^1\Sigma^+$, 1 $^1\Delta$, and 2 $^1\Pi$
C(^{3}P)–H$^+$(^{1}S)	1 $^3\Sigma^-$ and 2 $^3\Pi$
C$^+$(^{2}P)–H(^{2}S)	X $^1\Sigma^+$, A $^1\Pi$, a $^3\Pi$, and 1 $^3\Sigma^+$

transport collision integrals. Section III discusses the corresponding results. Finally, a conclusion is drawn in Sec. IV.

II. THEORY AND METHODS

A. *Ab initio* calculations of potential energy curves

For CH$^+$, PECs of 13 electronic states, including the X $^1\Sigma^+$, A $^1\Pi$, 2 $^1\Sigma^+$, 1 $^1\Delta$, 2 $^1\Pi$, a $^3\Pi$, 1 $^3\Sigma^+$, 1 $^3\Sigma^-$, 2 $^3\Pi$, 2 $^3\Sigma^-$, 3 $^3\Pi$, 1 $^5\Sigma^-$, and 1 $^5\Pi$ states, correlating with the first four dissociation channels were calculated with the MOLPRO 2015 quantum chemistry package.[60,61] The PECs are obtained using the state-averaged complete active space self-consistent field (SA-CASSCF) approach,[62,63] followed by internally contracted multireference configuration interaction method with the Davidson correction (icMRCI+Q),[64–67] which is widely used to study the PECs of diatomic molecules.[68–72] CH$^+$ belongs to the $C_{\infty v}$ symmetry. Our calculation of the PECs for CH$^+$ is performed in its largest Abelian subgroup (C_{2v}) because MOLPRO cannot deal with the non-Abelian (such as $C_{\infty v}$) symmetry.

The irreducible representation of the C_{2v} point group is (A_1, B_1, B_2, and A_2), and its corresponding relationship to the $C_{\infty v}$ point group can be described as follows: $\Sigma^+ \rightarrow A_1$, $\Sigma^- \rightarrow A_2$, $\Pi \rightarrow (B_1, B_2)$, $\Delta \rightarrow (A_1, A_2)$. To calculate the PECs for singlet and triplet electronic states, the
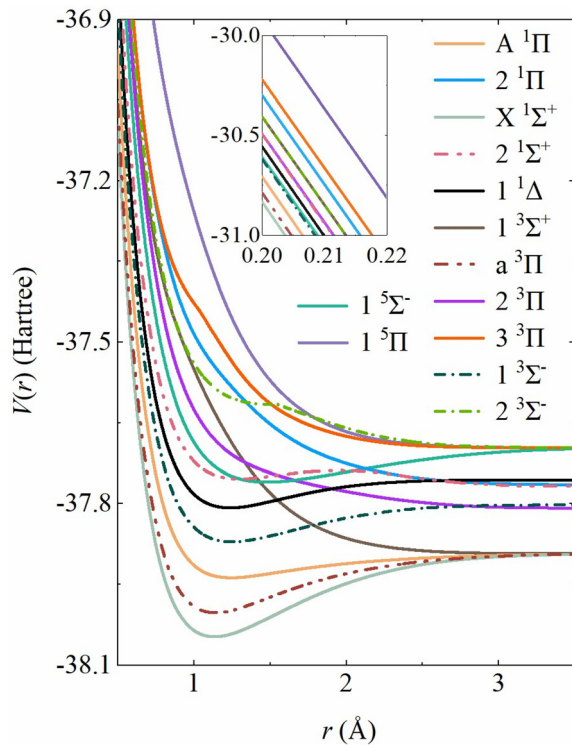

FIG. 1. Potential energy curves of CH$^+$ calculated using the icMRCI method with the aug-cc-pwCV5Z-DK basis set for the C atom/ion and the aug-cc-pV5Z basis set for the H atom/ion.
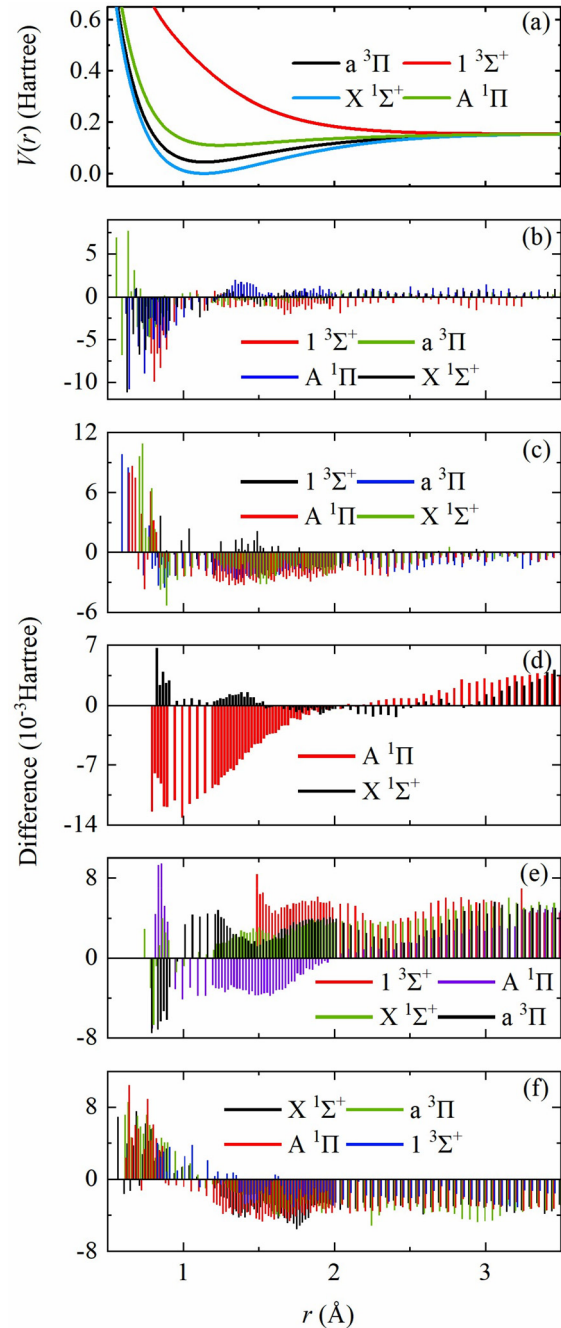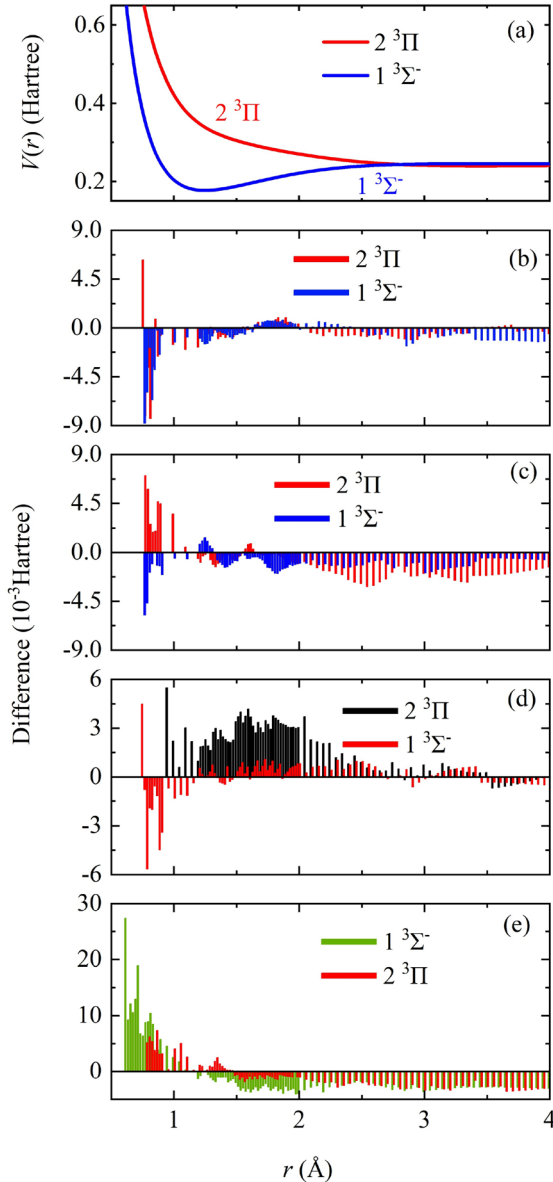

FIG. 2. Panel (a) represents our PECs for CH$^+$ correlating with the C$^+$(^{2}P)–H(^{2}S) dissociation limit. The differences between our PECs and those from Biglari *et al.*,[81] Mbiba Touedebe *et al.*,[82] Saxon *et al.*,[83] Green *et al.*,[84] and Liu *et al.*[24] are shown in panels (b)–(f), respectively.

electrons in the 1 s shell of C are put into one closed-shell orbital with one a_1 orbital, no b_1 orbital, b_2 orbital, and a_2 orbital. The remaining four electrons are placed into 11 outermost MOs, which constitute the active space: five a_1 orbitals, three b_1 orbitals, three b_2 orbitals, and no a_2 orbital. The orbitals of active space are called (5, 3, 3, 0). For the calculation of the PECs for quintet states, one MOs (1, 0, 0, 0) is kept closed in the reference space, and an extra two a_1 orbitals are added in the active space to describe the excited quintet states. The aug-cc-pwCV5Z-DK basis set is selected for describing the C atom/ion,
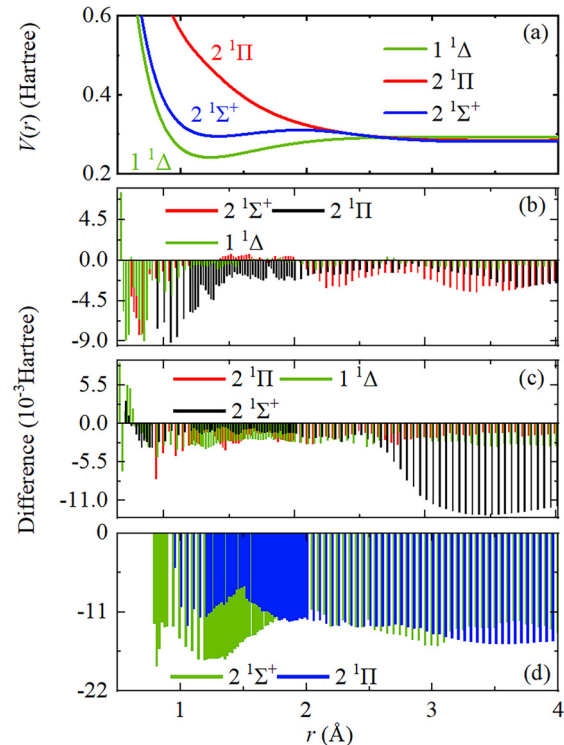
considering the core-valence (CV) correction. The aug-cc-pV5Z basis set is adopted for representing the H atom/ion. Scalar relativistic energy correction was calculated via the third-order Douglas–Kroll–Hess (DKH3) Hamiltonian approximation[73–75] at the icMRCI level of theory. The basis-set extrapolation is not considered in this work. The PECs of singlet electronic states were computed at the internuclear distances from 0.2 to 9.5 Å with step sizes of 0.05 Å for 0.2–0.4, 0.9–1.2, and 2–4 Å, 0.02 Å for 0.4–0.9 and 1.2–2 Å, 0.1 Å for 4–5 Å, and 0.5 Å for 5–9.5 Å. The PECs of triplet electronic states were computed at the internuclear distances from 0.2 to 9.5 Å with step sizes of 0.05 Å for 0.2–0.3, 0.9–1.2, and 2–4 Å, 0.02 Å for 0.3–0.9 and 1.2–2 Å, 0.1 Å for 4–5 Å, and 0.5 Å for 5–9.5 Å. The PECs for quintet states were computed at the internuclear distances from 0.2 to 9.5 Å with step sizes of 0.05 Å for 0.2–1.2 and 2–4 Å, 0.02 Å for 1.2–2 Å, 0.1 Å for 4–5 Å, and 0.5 Å for 5–9.5 Å.

For the calculation of collision integrals, *ab initio* potential energy points need to be extrapolated over the short and long ranges of internuclear distance r. In this work, the potential energy points were extrapolated by the following function for the short-range region at $R < 0.2$ Å:

$$V(r) = A \exp(-Br) + C, \tag{1}$$

where A, B, and C are fitting parameters. The cubic spline was used to interpolate the *ab initio* points. The total root mean square (RMS) errors of the cubic spline interpolation functions to *ab initio* potential

FIG. 3. Panel (a) represents our PECs for CH$^+$ correlating with the C(^{3}P)–H$^+$(^{1}S) dissociation limit. The differences between our PECs and those from Biglari *et al.*,[81] Mbiba Touedebe *et al.*,[82] Schultz and Krstić,[22] and Liu *et al.*[24] are shown in panels (b)–(e), respectively.

FIG. 4. Panel (a) represents our PECs for CH$^+$ correlating with the C(^{1}D)–H$^+$(^{1}S) dissociation limit. The differences between our PECs and those from Biglari *et al.*,[81] Mbiba Touedebe *et al.*,[82] and Saxon *et al.*[83] are shown in panels (b)–(d), respectively.

energy points do not exceed 10^{-7} cm^{-1}. To ensure continuous and smooth PECs, the long-range region at $R > 9.5$ Å was extrapolated by the following function:

$$V(r) = -\frac{C_5}{R^5} - \frac{C_7}{R^7} + V(r \to \infty), \qquad (2)$$

where C_5 and C_7 are state-dependent coefficients, which were estimated by fitting *ab initio* points. The fitting parameters to PECs of CH$^+$ in Eqs. (1) and (2) are listed in Tables IV and V in the Appendix.

B. Quantum and classical approaches for determining cross sections

A quantum mechanical description of the scattering with WKB approximations to the scattering phase shifts was used to obtain transport cross sections. The quantum mechanical cross sections[76] related to transport properties, such as diffusion coefficient and viscosity coefficient, are MTCS,

$$Q^{(1)}(E) = \frac{4\pi}{k^2} \sum_{l=0}^{\infty} (l+1) \sin^2(\delta_l - \delta_{l+1}), \qquad (3)$$

and VCS,

$$Q^{(2)}(E) = \frac{4\pi}{k^2} \sum_{l=0}^{\infty} \frac{(l+1)(l+2)}{2l+3} \sin^2(\delta_l - \delta_{l+2}), \qquad (4)$$

and the third moment cross section $Q^{(3)}$ is as follows:
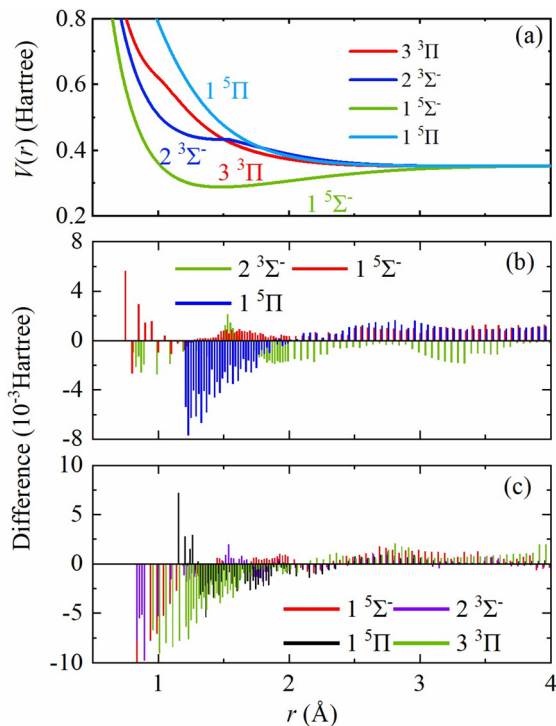
FIG. 5. Panel (a) represents our PECs for CH$^+$ correlating with the C$^+$(^{4}P)–H(^{2}S) dissociation limit. The differences between our PECs and those from Biglari *et al.*[81] and Mbiba Touedebe *et al.*[82] are shown in panels (b) and (c), respectively.

$$Q^{(3)}(E) = \frac{4\pi}{k^2} \sum_{l=0}^{\infty} \left[\frac{3(l+1)(l^2+2l-1)}{(2l-1)(2l+5)} \sin^2(\delta_l - \delta_{l+1}) + \frac{(l+1)(l+2)(l+3)}{(2l+3)(2l+5)} \sin^2(\delta_l - \delta_{l+3}) \right], \qquad (5)$$

where δ_l is the scattering phase shift related to the lth partial wave, $k = \sqrt{2\mu E}$, E is the collision energy, and μ is the reduced mass of the interacting atoms. The scattering phase shifts δ_l can be obtained from the WKB approximation,

$$\delta_l(E) = k \lim_{r' \to \infty} \left(\int_{r_c}^{r'} \sqrt{1 - \frac{V(r)}{E} - \frac{(l+1/2)^2}{k^2 r^2}} \, dr \right. $$
$$\left. - \int_{(l+1/2)/k}^{r'} \sqrt{1 - \frac{(l+1/2)^2}{k^2 r^2}} \, dr \right), \qquad (6)$$

TABLE III. Comparison of spectroscopic constants for electronic states of CH$^+$.

State	Ref.	T_e (cm^{-1})	D_e (cm^{-1})	r_e(Å)
X $^1\Sigma^+$	This work	0.0	34 333.0835	1.13
	Exp.	0.0	34 363[a]	1.130 88[b]
	Ref. 81	0.0	342 27	1.13
	Ref. 83	0.0	333 91	1.129
	Ref. 85	0.0	· · ·	1.1404
	Ref. 86	0.0	37 585	1.1250
A $^1\Pi$	This work	24 193.4216	10 167.6752	1.23
	Exp.	24 119[b]	10 308[b]	1.23 505[b]
	Ref. 81	24 236	9992	1.239
	Ref. 85	23 366	· · ·	1.3118
	Ref. 86	· · ·	12 340	1.2055
1 $^1\Delta$	This work	52 737.4055	10 860.0761	1.23
	Exp.	52 534[c]	10 865[c]	1.2325[c]
	Ref. 81	52 897	10 815	1.234
	Ref. 85	53 016	· · ·	1.2864
	Ref. 86	· · ·	12 663	1.2086
a $^3\Pi$	This work	9808.3827	24 497.2990	1.13
	Exp.	· · ·	· · ·	1.1348[d]
	Ref. 81	9708	24 519	1.135
	Ref.85	8804	· · ·	1.1473
	Ref. 86	· · ·	27 745	1.1261
1 $^3\Sigma^-$	This work	39 408.7770	14 741.6840	1.25
	Exp.	· · ·	· · ·	1.2416[d]
	Ref. 81	38 689	14 783	1.244
	Ref. 85	36 681	· · ·	1.2954
1 $^5\Sigma^-$	This work	66 820.0457	14 258.9846	1.47
	Ref. 81	63 058	14 241	1.477
	Ref. 85	58 608	· · ·	1.5018

[a]Ref. 88.
[b]Ref. 87.
[c]Ref. 89.
[d]Ref. 90.

where $V(r)$ is the potential energy function describing interatomic interaction, E is the collision energy, and r_c is the classical turning point, namely, the distance of the closest approach.

In classical mechanics, the cross sections are expressed by integrating over the impact parameter b,

$$Q^{(n)}(E) = 2\pi \int_0^\infty b(1 - \cos^n[\chi(b, E)])\mathrm{d}b, \tag{7}$$

with the deflection angle

$$\chi(b, E) = \pi - 2b \int_{r_c}^\infty \frac{\mathrm{d}r}{r^2\sqrt{1 - \dfrac{b^2}{r^2} - \dfrac{V(r)}{E}}}. \tag{8}$$

If two particles interact according to more than one PEC, the transport cross section is defined as the weighted average,[23,77]

$$Q_{av}^l(E) = \frac{\sum\limits_i w_i Q_i^l(E)}{\sum\limits_i w_i}, \tag{9}$$

where w_i are the statistical weights according to molecular term symbols[78–80] and listed in Table I. $Q_i^l(E)$ is the (CM or QM-WKB) transport cross sections associated with each dissociation limit at the ith electronic state.

From the (CM or QM-WKB) transport cross sections, the reduced transport collision integrals can be calculated by

$$\sigma^2 \Omega_{av}^{(l,s)*} = \frac{1}{(k_B T)^{s+2} \pi (s+1)! \left[1 - \dfrac{1}{2}\dfrac{1 + (-1)^l}{1 + l}\right]}$$
$$\times \int_0^\infty e^{-E/(k_B T)} E^{s+1} Q_{av}^l(E)\,dE. \tag{10}$$

III. RESULTS AND DISCUSSION

In this work, 13 electronic states of CH^+ are considered and shown in Table II, together with their corresponding dissociation limits. Figure 1 shows the computed PECs of these 13 electronic states. There exist four electronic states correlating with the $C^+(^2P)$–$H(^2S)$ dissociation limit, including the X $^1\Sigma^+$, A $^1\Pi$, a $^3\Pi$, and 1 $^3\Sigma^+$ states. It is worth noting that the 1 $^3\Sigma^+$ state is repulsive while the X $^1\Sigma^+$, A $^1\Pi$, and a $^3\Pi$ states possess potential wells of varying depths. The 1 $^3\Sigma^-$ state is bound with a potential well of about 0.07 hartree, the 2 $^3\Pi$ state is repulsive, and both states converge to the $C(^3P)$–$H^+(^1S)$ asymptote. The 2 $^1\Sigma^+$, 1 $^1\Delta$, and 2 $^1\Pi$ states correlate with the $C(^1D)$–$H^+(^1S)$ dissociation limit. The 1 $^1\Delta$ state possesses a potential well of about 0.05 hartree, and the 2 $^1\Pi$ state is repulsive, while the 2 $^1\Sigma^+$ state presents a potential well and a potential barrier emerges
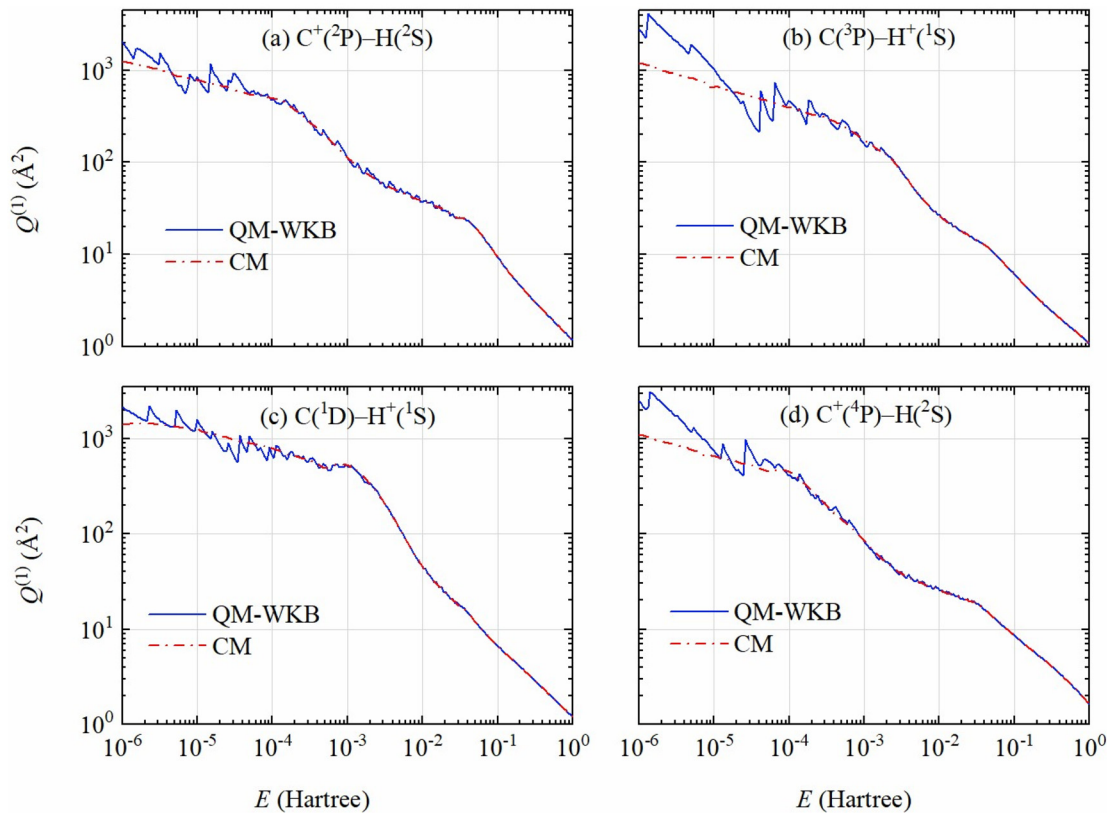

FIG. 6. MTCS $Q^{(1)}$ for the (a) $C^+(^2P)$–$H(^2S)$, (b) $C(^3P)$–$H^+(^1S)$, (c) $C(^1D)$–$H^+(^1S)$, and (d) $C^+(^4P)$–$H(^2S)$ interactions obtained by the QM-WKB and CM methods.
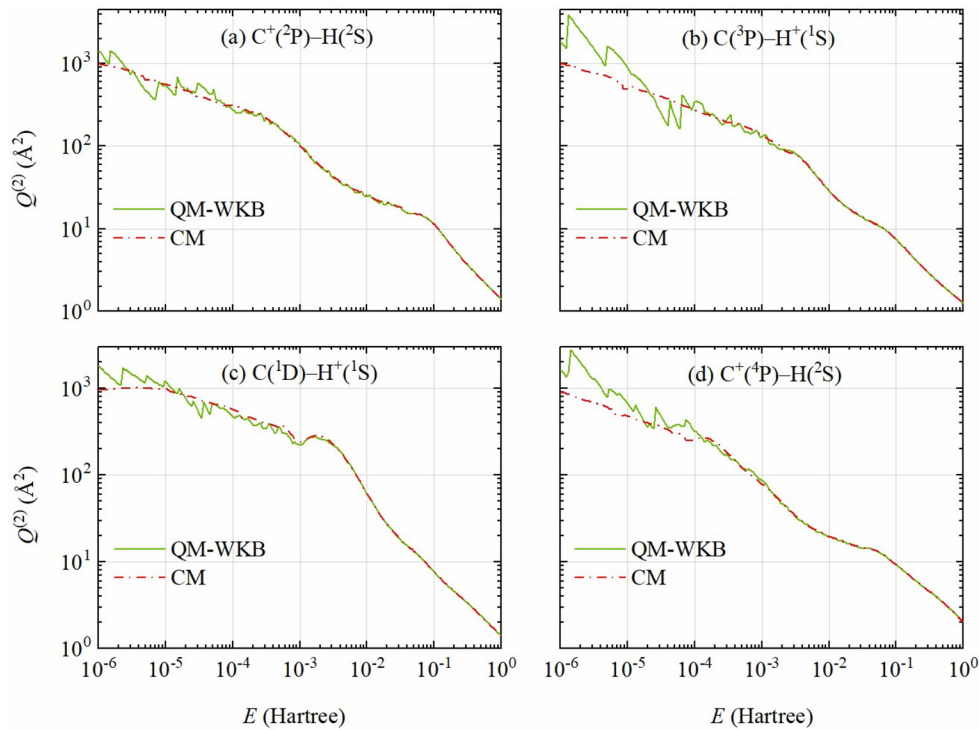
FIG. 7. VCS $Q^{(2)}$ for the (a) $C^+(^2P)$–$H(^2S)$, (b) $C(^3P)$–$H^+(^1S)$, (c) $C(^1D)$–$H^+(^1S)$, and (d) $C^+(^4P)$–$H(^2S)$ interactions obtained by the QM-WKB and CM methods.
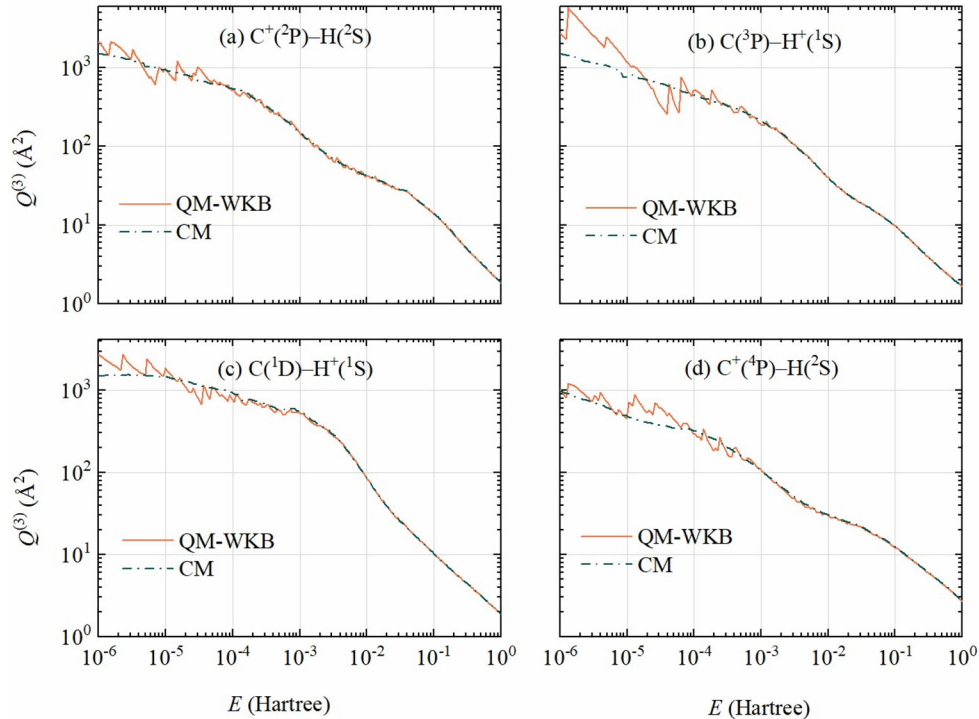

FIG. 8. The third moment cross section $Q^{(3)}$ for the (a) $C^+(^2P)$–$H(^2S)$, (b) $C(^3P)$–$H^+(^1S)$, (c) $C(^1D)$–$H^+(^1S)$, and (d) $C^+(^4P)$–$H(^2S)$ interactions obtained by the QM-WKB and CM methods.
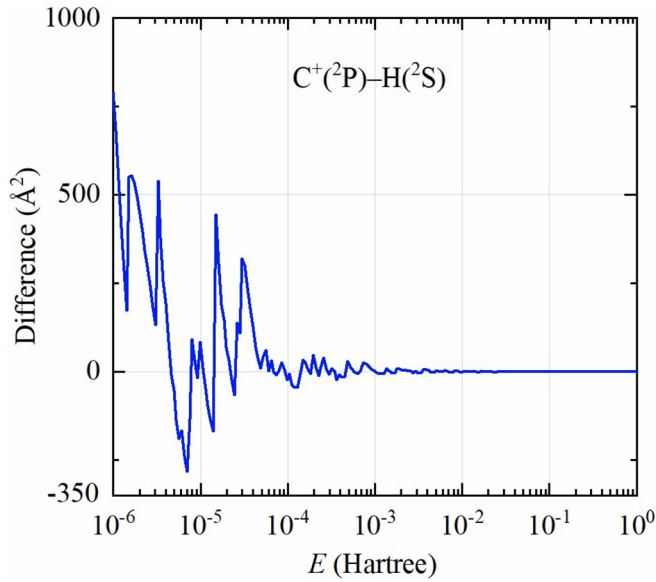
25 October 2023 11:56:47

FIG. 9. The difference between MTCSs for the $C^+(^2P)$–$H(^2S)$ interaction obtained by the QM-WKB and CM methods.

above its dissociation limit. There are four electronic states that converge to the $C^+(^4P)$–$H(^2S)$ asymptote, including the $2\,^3\Sigma^-$, $3\,^3\Pi$, $1\,^5\Sigma^-$, and $1\,^5\Pi$ states. The $1\,^5\Sigma^-$ state has a potential well of about 0.07 hartree, while the $2\,^3\Sigma^-$, $3\,^3\Pi$, and $1\,^5\Pi$ states are repulsive. Our calculated maximum *ab initio* potential energies of the 13 electronic states lie at 0.2 Å and are more than 7 hartree above their dissociation limits, which enables accurate calculation of transport cross sections and transport collision integrals.

Comparisons between our PECs correlating with the first four dissociation channels of CH^+ and those computed by other researchers are made to verify the reliability of our *ab initio* data, which are shown in Figs. 2–5. Panel (a) of Figs. 2–5 represent our PECs calculated using the icMRCI method with the aug-cc-pwCV5Z-DK basis set for the C atom/ion and the aug-cc-pV5Z basis set for the H atom/ion. Panel (b) of Figs. 2–5 represents the differences between PECs calculated by Biglari *et al.*[81] using the MRCI method with the cc-pV5Z basis set and our PECs. Panel (c) of Figs. 2–5 shows the differences between PECs calculated by Mbiba Touedebe *et al.*[82] using the MRCI method with the cc-pV6Z basis set and our PECs. Panel (d) of Figs. 2 and 4 represents the differences between PECs computed by Saxon *et al.*[83] using the configuration interaction (CI) method and the extended Slater-type basis and our PECs. Panel (d) of Fig. 2 represents the differences between PECs calculated by Green *et al.*[84] in the CI calculations
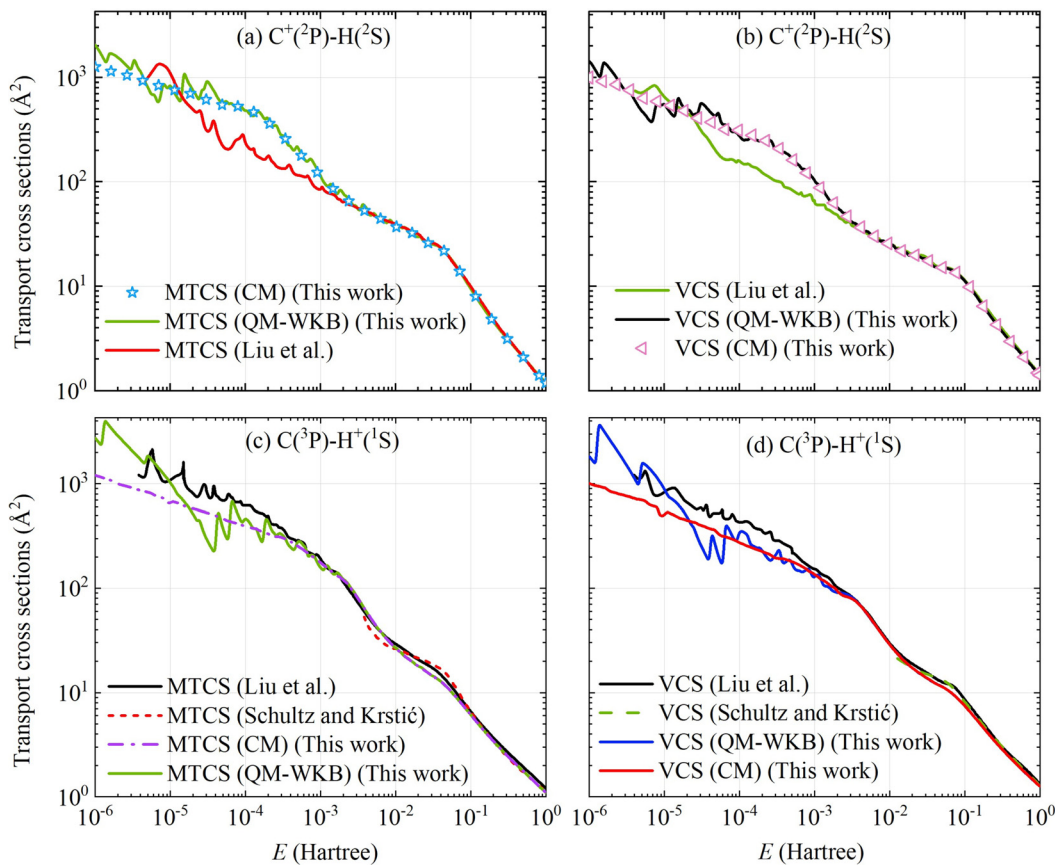

FIG. 10. Comparison of the transport cross sections for the (a) $C^+(^2P)$–$H(^2S)$ and (b) $C(^3P)$–$H^+(^1S)$ interactions obtained in this work with those from Schultz and Krstić[22] and Liu *et al.*[24]

with the Slater-type basis and our PECs. Panel (f) of Fig. 2 and panel (e) of Fig. 3 represent the differences between PECs computed by Liu *et al.*[24] using the multireference single- and double-excitation configuration interaction (MRD-CI) method with the cc-pVQZ basis set and our PECs. Panel (d) of Fig. 3 shows the differences between PECs calculated by Schultz and Krstić[22] using the MRD-CI method with the atomic orbital basis sets that consisted of contracted Cartesian Gaussian functions. The PECs of these 13 electronic states of CH^+ show reasonable agreement with previous calculations,[81–84] especially the more recent ones, except for those of the 2 $^1\Pi$ and 2 $^1\Sigma^+$ states obtained by Saxon *et al.*,[83] and 1 $^3\Sigma^-$ state from Liu *et al.*,[24] which may result from the difference in the optimization of orbitals or different basis sets adopted. The spectroscopic constants computed in the present work are compared with those of the previous studies[81,83,85,86] and with the experimental values[87–90] in Table III. Our adiabatic excitation energy (T_e) and dissociation energy (D_e) for X $^1\Sigma^+$, A $^1\Pi$, and

1 $^1\Delta$ states are closer to the experimental values. The equilibrium internuclear distance (r_e) for the X $^1\Sigma^+$, A $^1\Pi$, a $^3\Pi$, 1 $^1\Delta$, 1 $^3\Sigma^-$, and 1 $^5\Sigma^-$ states shows reasonable agreement with previous calculations. Overall, our *ab initio* PECs of CH^+ are reliable and can be used to calculate the corresponding transport collision integrals.

The obtained PECs of CH^+ were used to calculate the transport cross sections for the $C^+(^2P)–H(^2S)$, $C(^3P)–H^+(^1S)$, $C(^1D)–H^+(^1S)$, and $C^+(^4P)–H(^2S)$ interactions using QM-WKB and CM methods, which are shown in Figs. 6–8 for MTCS $Q^{(1)}$, VCS $Q^{(2)}$, and the third moment cross section $Q^{(3)}$, respectively. The transport cross sections computed by the QM-WKB and CM methods are nearly identical in the high collision energy regions. For example, the MTCSs for the $C(^3P)–H^+(^1S)$ interaction obtained by the QM-WKB method are almost the same as those obtained by the CM method in the collision energy of 0.02–1 hartree. The transport cross sections obtained by the QM-WKB method oscillate around ones determined from the CM method
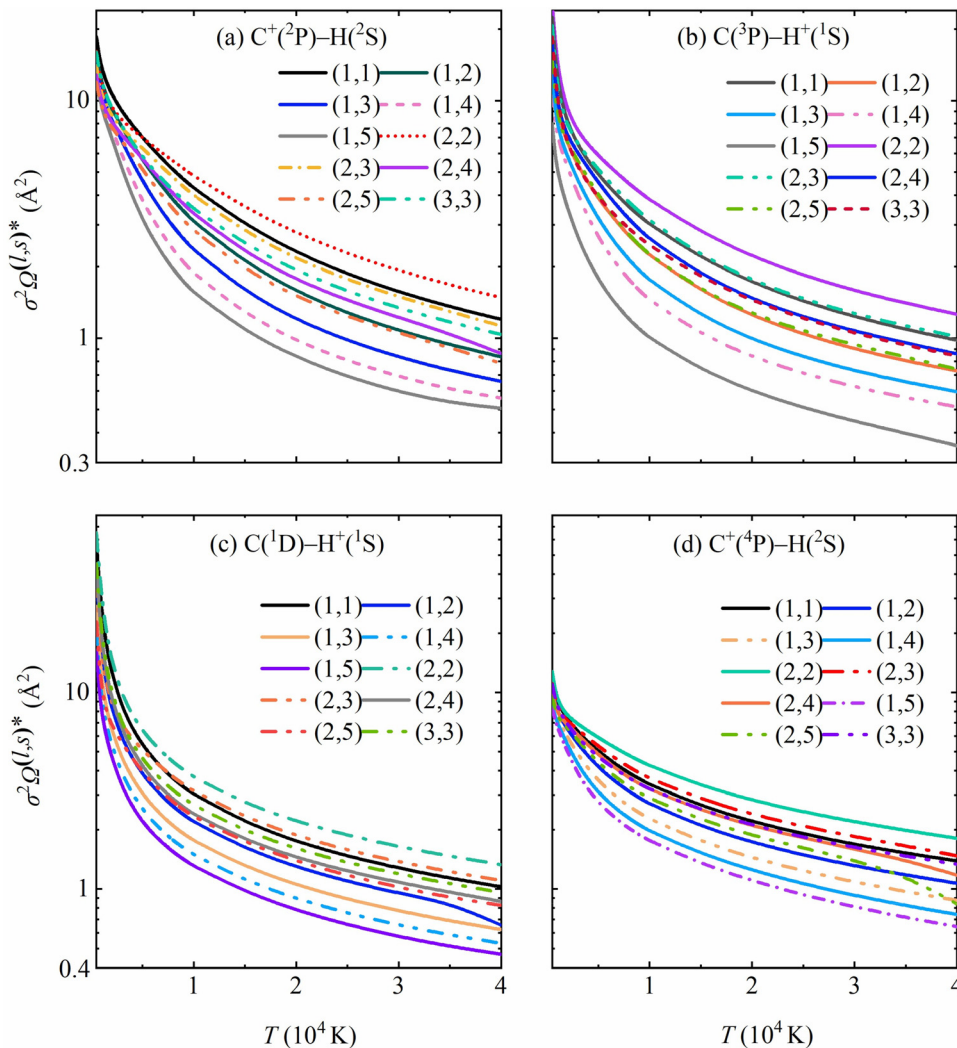

FIG. 11. Transport collision integrals of the (a) $C^+(^2P)–H(^2S)$, (b) $C(^3P)–H^+(^1S)$, (c) $C(^1D)–H^+(^1S)$, and (d) $C^+(^4P)–H(^2S)$ interactions calculated with the QM-WKB method.

in the low collision energy regions. For collision energies below about 4.5×10^{-5} hartree, the QM-WKB transport cross sections show more significant deviations from the CM results. For example, the MTCS for the $C(^3P)$–$H^+(^1S)$ interaction obtained by the QM-WKB method is about twice that obtained by the CM method at the considered lowest energy of 10^{-6} hartree. Figure 9 shows an example of the differences between MTCSs for the $C^+(^2P)$–$H(^2S)$ interaction obtained by both methods. As shown, there are slight differences in the high collision energy regions and huge differences in the low collision energy regions. The transport cross sections are not only influenced by the transport cross sections of related electronic states, but also influenced by the number of electronic (both bound and repulsive) states, and their statistical weights correlating with their dissociation limits.

Figure 10 shows the comparisons between our transport cross sections for the $C^+(^2P)$–$H(^2S)$, $C(^3P)$–$H^+(^1S)$ interactions and those computed by other researchers.[22,24] Our transport cross sections for the $C^+(^2P)$–$H(^2S)$ interaction are close to those from Schultz and Krstić,[22] and Liu *et al.*[24] in the collision energy of 0.04–1 hartree as shown in Fig. 10. Differences are visible between the transport cross sections for the $C^+(^2P)$–$H(^2S)$, $C(^3P)$–$H^+(^1S)$ interactions obtained in this work and those from Schultz and Krstić,[22] and Liu *et al.*[24] in the low collision energy ranges, which may be caused by the different methods of calculating transport cross sections and the difference of PECs.

The transport cross sections for the $C^+(^2P)$–$H(^2S)$, $C(^3P)$–$H^+(^1S)$, $C(^1D)$–$H^+(^1S)$, and $C^+(^4P)$–$H(^2S)$ interactions were used to calculate the transport collision integrals over the temperature range of 500–40 000 K. Figure 11 shows transport collision integrals for the $C^+(^2P)$–$H(^2S)$, $C(^3P)$–$H^+(^1S)$, $C(^1D)$–$H^+(^1S)$, and $C^+(^4P)$–$H(^2S)$ interactions computed with the QM-WKB method, and Fig. 12
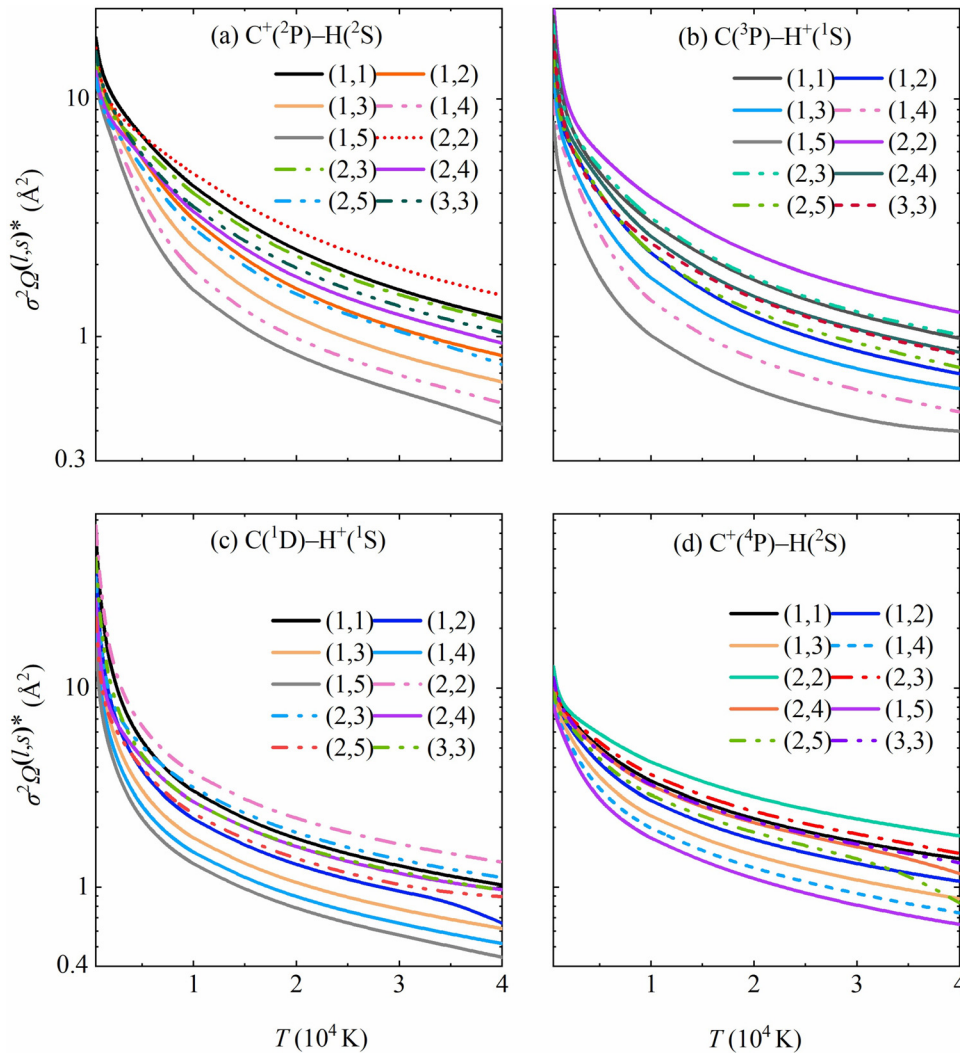

FIG. 12. Transport collision integrals of the (a) $C^+(^2P)$–$H(^2S)$, (b) $C(^3P)$–$H^+(^1S)$, (c) $C(^1D)$–$H^+(^1S)$, and (d) $C^+(^4P)$–$H(^2S)$ interactions calculated with the CM method.
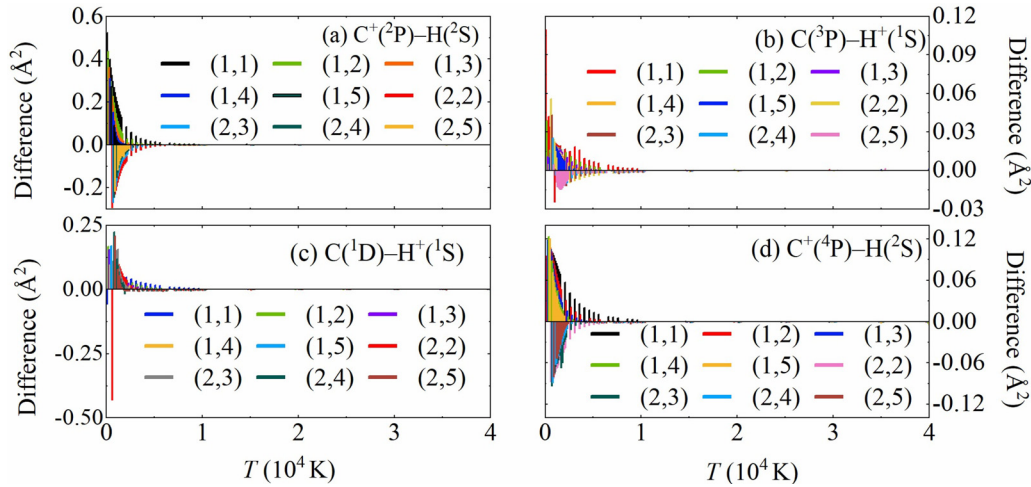
FIG. 13. Differences of transport collision integrals for the (a) $C^+(^2P)$–$H(^2S)$, (b) $C(^3P)$–$H^+(^1S)$, (c) $C(^1D)$–$H^+(^1S)$, and (d) $C^+(^4P)$–$H(^2S)$ interactions between the QM-WKB and CM methods.

displays those calculated with the CM method. All transport collision integrals decrease with increasing temperature over the whole temperature range considered here. The QM-WKB and CM methods produce significantly different transport cross sections in the low collision energy regions, while the resulting transport collision integrals are very similar. All the discrepancies between the transport collision integrals obtained using QM-WKB and CM methods are less than 1% in the temperature range of about 2500–40 000 K except for $\sigma^2\Omega^{(3,3)*}$ of the $C^+(^2P)$–$H(^2S)$ interaction. The maximum deviation for $\sigma^2\Omega^{(3,3)*}$ of $C^+(^2P)$–$H(^2S)$ interaction obtained using QM-WKB and CM methods is 3.22% at 500 K. Figure 13 presents the differences of transport collision integrals for the $C^+(^2P)$–$H(^2S)$, $C(^3P)$–$H^+(^1S)$, $C(^1D)$–$H^+(^1S)$, and $C^+(^4P)$–$H(^2S)$ interactions between the QM-WKB and CM methods. There are larger differences of the transport collision integrals obtained using QM-WKB and CM methods in low-temperature ranges, which may be caused by the different transport cross sections obtained by the QM-WKB and CM methods in the low collision energy regions. The discrepancies of the transport collision integrals obtained using those two methods are getting smaller with increasing temperature. Buchowiecki and Szabó[41] pointed out that the maximum difference of transport collision integrals computed using the CM method introduced by various PECs, such as HH, MS, and *ab initio* PECs, may exceed 20%, which means that the inaccuracy of transport collision integrals introduced by the QM-WKB and CM approaches is possibly smaller than the that introduced by the PECs. Detailed data on our calculated transport collision integrals are given in the supplementary material.

Here, we take the collision between carbon atoms and H ions as an example to explain the effect of the excited states on the transport properties. It is assumed that the C atoms and H ions in a plasma mixture with a certain pressure are in thermodynamic equilibrium and their numbers in ground and excited states satisfy the Boltzmann distribution equation. Carbon atoms in ground and excited states as a proportion of the total number of carbon atoms can be estimated at a temperature of T,

$$n_i = n_T \frac{g_i}{Z(T)} e^{-E_i/k_B T}, \tag{11}$$

where n_i is the number density of ith atomic excited state, g_i is the degeneracy of ith atomic excited state, E_i is the energy of ith atomic excited state, n_T is the total number density of atomic carbon, and $Z(T)$ is the electronic partition function of carbon atoms. At 40 000 K, the number of carbon atoms in the first excited state constitutes 19% of the total carbon atoms ($n_1 = 0.19n_T$). The excitation of hydrogen ions can be ignored in the considered temperature range. Based on the predicted numbers of C in ground and excited states, the percentage of the contributions of transport collision integrals $\sigma^2\Omega^{(1,1)*}$ obtained using QM-WKB method for $C(^3P)$–$H^+(^1S)$ interaction at 4000 K is 98.69%, which is 1.31% for the $C(^1D)$–$H^+(^1S)$ interaction, whose sum is 100%. The percentages of the contributions of transport collision integrals $\sigma^2\Omega^{(1,1)*}$ for the $C(^3P)$–$H^+(^1S)$ and $C(^1D)$–$H^+(^1S)$ interactions at 10 000 K are 91.38% and 8.62%, respectively. At 40 000 K, the percentages of the contributions of transport collision integrals $\sigma^2\Omega^{(1,1)*}$ for the $C(^3P)$–$H^+(^1S)$ interaction dropped to 78.76%, which is up to 21.24% for the $C(^1D)$–$H^+(^1S)$ interaction. Therefore, transport collision integrals of the interactions between the atomic/ionic ground and excited states should not be ignored in plasma modeling at high temperatures.

IV. CONCLUSIONS

In this work, we have used the QM-WKB and CM methods to carry out a comprehensive theoretical investigation of the transport cross sections and transport collision integrals for the $C^+(^2P)$–$H(^2S)$, $C(^3P)$–$H^+(^1S)$, $C(^1D)$–$H^+(^1S)$, and $C^+(^4P)$–$H(^2S)$ interactions based on the extrapolated *ab initio* PECs of 13 electronic states over the temperature range of 500–40 000 K. The $C(^1D)$–$H^+(^1S)$, and $C^+(^4P)$–$H(^2S)$ interactions are considered for the first time. The PECs of CH^+ are obtained using the icMRCI+Q method with the aug-cc-pwCV5Z-DK basis set for the C atom/ion and the aug-cc-pV5Z basis set for the H atom/ion and are then compared with those computed by other

TABLE IV. The fitting parameters to PECs of CH$^+$ in Eq. (1).

State	A (10^6)	B	C	State	A (10^6)	B	C
X $^1\Sigma^+$	8.351 366	9.000 043	168 850.817	1 $^1\Delta$	8.037 792	8.772 560	190 404.264
A $^1\Pi$	8.212 616	8.914 629	195 977.013	2 $^1\Pi$	8.409 095	9.266 317	319 261.385
a $^3\Pi$	8.302 057	8.956 658	175 057.465	2 $^3\Sigma^-$	8.306 408	9.217 285	285 172.984
1 $^3\Sigma^+$	8.307 786	9.218 960	328 597.580	3 $^3\Pi$	8.009 288	8.911 096	292 897.207
1 $^3\Sigma^-$	8.104 211	8.833 373	191 951.962	1 $^5\Sigma^-$	8.281 009	9.231 146	248 269.326
2 $^3\Pi$	8.403 502	9.306 602	298 424.300	1 $^5\Pi$	8.277 381	9.119 653	370 862.305
2 $^1\Sigma^+$	8.014 863	8.774 219	208 444.841				

researchers to verify the reliability of our *ab initio* PECs, which shows that our *ab initio* PECs are reliable. The resulting transport cross sections and transport collision integrals are of great importance for computing the transport properties of high-temperature plasmas involving C and H atoms/ions.

SUPPLEMENTARY MATERIAL

See the supplementary material for details of transport collision integrals.

ACKNOWLEDGMENTS

AUTHOR DECLARATIONS
Conflict of Interest

The authors have no conflicts to disclose.

Author Contributions

Zhenlu Hou: Formal analysis (equal); Investigation (equal); Writing – original draft (equal). **Zhi Qin:** Conceptualization (equal); Funding acquisition (equal); Methodology (equal); Supervision (equal); Writing – review & editing (equal). **Linhua Liu:** Funding acquisition (equal); Supervision (equal); Writing – review & editing (equal).

DATA AVAILABILITY

The data that support the findings of this study are available within the article and its supplementary material.

APPENDIX: THE FITTING PARAMETERS TO PECS

The fitting parameters to PECs of CH$^+$ in Eqs. (1) and (2) are shown in Tables IV and V, respectively. The units of $V(r)$ in Eqs. (1) and (2) are cm^{-1}.

TABLE V. The fitting parameters to PECs of CH$^+$ in Eq. (2).

State	C_5 (10^5)	C_7 (10^7)	State	C_5 (10^5)	C_7 (10^7)
X $^1\Sigma^+$	−4.626 885	41.641 96	1 $^1\Delta$	0.442 711 0	−3.984 399
A $^1\Pi$	−8.020 060	72.180 54	2 $^1\Pi$	−40.056 57	360.5092
a $^3\Pi$	−1.368 664	12.317 98	2 $^3\Sigma^-$	−0.151 611 2	1.364 500
1 $^3\Sigma^+$	0.068 060 09	0.612 540 8	3 $^3\Pi$	−0.068 444 61	0.616 001 5
1 $^3\Sigma^-$	0.588 113 3	−5.293 019	1 $^5\Sigma^-$	−2.029 053	18.261 48
2 $^3\Pi$	−2.352 907	21.176 16	1 $^5\Pi$	−1.557 744	14.019 69
2 $^1\Sigma^+$	−36.812 74	331.3147			

REFERENCES

[1] E. Habart, E. Dartois, A. Abergel, J.-P. Baluteau, D. Naylor, E. Polehampton, C. Joblin, P. Ade, L. Anderson, and P. André, "SPIRE spectroscopy of the prototypical Orion Bar photodissociation region," Astron. Astrophys. **518**, L116 (2010).

[2] A. Douglas and G. Herzberg, "Note on CH$^+$ in interstellar space and in the laboratory," Astrophys. J. **94**, 381 (1941).

[3] L. Hobbs, J. Thorburn, T. Oka, J. Barentine, T. Snow, and D. York, "Atomic and molecular emission lines from the red rectangle," Astrophys. J. **615**, 947 (2004).

[4] J. Cernicharo, X.-W. Liu, E. González-Alfonso, P. Cox, M. Barlow, T. Lim, and B. Swinyard, "Discovery of far-infrared pure rotational transitions of CH$^+$ in NGC 7027," Astrophys. J. **483**, L65 (1997).

[5] E. Falgarone, V. Ossenkopf, M. Gerin, P. Lesaffre, B. Godard, J. Pearson, S. Cabrit, C. Joblin, A. O. Benz, and F. Boulanger, "Strong CH$^+$ $J = 1$-0 emission and absorption in DR21," Astron. Astrophys. **518**, L118 (2010).

[6] W.-F. Thi, F. Ménard, G. Meeus, C. Martin-Zaïdi, P. Woitke, E. Tatulli, M. Benisty, I. Kamp, I. Pascucci, and C. Pinte, "Detection of CH$^+$ emission from the disc around HD 100546," Astron. Astrophys. **530**, L2 (2011).

[7] B. Godard, E. Falgarone, M. Gerin, D. C. Lis, M. De Luca, J. H. Black, J. R. Goicoechea, J. Cernicharo, D. A. Neufeld, and K. M. Menten, "Comparative study of CH$^+$ and SH$^+$ absorption lines observed towards distant star-forming regions," Astron. Astrophys. **540**, A87 (2012).

[8] A. T. Myers, C. F. McKee, and P. S. Li, "The CH$^+$ abundance in turbulent, diffuse molecular clouds," Mon. Not. R. Astron. Soc. **453**, 2748 (2015).

[9] V. Valdivia, B. Godard, P. Hennebelle, M. Gerin, P. Lesaffre, and J. Le Bourlot, "Origin of CH$^+$ in diffuse molecular clouds-warm H$_2$ and ion-neutral drift," Astron. Astrophys. **600**, A114 (2017).

[10] P. André, J. Aubreton, S. Clain, M. Dudeck, E. Duffour, M.-F. Elchinger, B. Izrar, D. Rochette, R. Touzani, and D. Vacher, "Transport coefficients in thermal plasma. Applications to Mars and Titan atmospheres," Eur. Phys. J. D **57**, 227 (2010).

[11] D. Smith, "The ion chemistry of interstellar clouds," Chem. Rev. **92**, 1473 (1992).

[12]H. S. Müller, "Spectroscopic parameters and rest frequencies of isotopic methylidynium, CH^+," Astron. Astrophys. **514**, L6 (2010).

[13]H. Helm, P. Cosby, M. Graff, and J. Moseley, "Photofragment spectroscopy of CH^+: Laser excitation of shape resonances in the A $^1\Pi$ state," Phys. Rev. A **25**, 304 (1982).

[14]B. Godard and J. Cernicharo, "A complete model of CH^+ rotational excitation including radiative and chemical pumping processes," Astron. Astrophys. **550**, A8 (2013).

[15]R. Janev and D. Reiter, "Collision processes of CH_y and CH_y^+ hydrocarbons with plasma electrons and protons," Phys. Plasmas **9**, 4071 (2002).

[16]A. Mahfouf, P. André, G. Faure, and M.-F. Elchinger, "Theoretical and numerical study of transport collision integrals: Application to $O(^3P)$–$O(^3P)$ interaction," Chem. Phys. **491**, 1–10 (2017).

[17]H. Partridge, J. R. Stallcop, and E. Levin, "Transport cross sections and collision integrals for $N(^4S^o)$–$O^+(^4S^o)$ and $N^+(^3P)$–$O(^3P)$ interactions," Chem. Phys. Lett. **184**, 505 (1991).

[18]J. R. Stallcop, H. Partridge, and E. Levin, "Resonance charge transfer, transport cross sections, and collision integrals for $N^+(^3P)$–N $(^4S^0)$ and $O^+(^4S^0)$–$O(^3P)$ interactions," J. Chem. Phys. **95**, 6429 (1991).

[19]M. J. Wright, H. H. Hwang, and D. W. Schwenke, "Recommended collision integrals for transport property computations. Part II: Mars and Venus entries," AIAA J. **45**, 281 (2007).

[20]A. Murphy, "Transport coefficients of hydrogen and argon–hydrogen plasmas," Plasma Chem. Plasma Process. **20**, 279 (2000).

[21]W. Wang, "Investigation of the dynamic characteristics and decaying behaviour of SF_6 arcs in switching applications," Ph.D. thesis (The University of Liverpool, 2013).

[22]D. Schultz and P. Krstić, "Transport cross sections relevant to cool hydrogen plasmas bounded by graphite," Phys. Plasmas **9**, 64 (2002).

[23]B. Sourd, J. Aubreton, M.-F. Elchinger, M. Labrot, and U. Michon, "High temperature transport coefficients in e/C/H/N/O mixtures," J. Phys. D **39**, 1105 (2006).

[24]C. Liu, J. Wang, and R. Janev, "Elastic and related transport cross sections for singly charged ion–atom scattering involving H, Be and C atoms and their ions," J. Phys. B **43**, 144006 (2010).

[25]A. Sanon and J. Baronnet, "Transport coefficients of Ar/C/H/O/N systems thermal plasma at atmospheric pressure," IOP Conf. Ser.: Mater. Sci. Eng. **29**, 012003 (2012).

[26]W. Wang, J. D. Yan, M. Rong, A. Murphy, and J. W. Spencer, "Thermophysical properties of high temperature reacting mixtures of carbon and water in the range 400–30,000 K and 0.1–10 atm. Part 2: Transport coefficients," Plasma Chem. Plasma Process. **32**, 495 (2012).

[27]M. Buchowiecki and P. Szabó, "Collision integrals for nitrogen and hydrogen ionized gas: The exact values and assessment of approximations," Plasma Chem. Plasma Process. **43**, 449 (2023).

[28]M. Buchowiecki and P. Szabó, "On the usefulness of the classical description of collision integrals of interacting atoms/ions. Collision integrals for O (^3P)–O (^3P) interaction," https://ssrn.com/abstract=4423096 (2023).

[29]L. S. Tee, S. Gotoh, and W. E. Stewart, "Molecular parameters for normal fluids. Lennard-Jones 12-6 potential," Ind. Eng. Chem. Fundam. **5**, 356 (1966).

[30]X. Wang, S. Ramírez-Hinestrosa, J. Dobnikar, and D. Frenkel, "The Lennard-Jones potential: When (not) to use it," Phys. Chem. Chem. Phys. **22**, 10624 (2020).

[31]R. Zhou, Z. Qiu, C. Sun, and B. Bai, "Entrance loss of capillary flow in narrow slit nanochannels," Phys. Fluids **35**, 042005 (2023).

[32]S. Kazem Manzoorolajdad, H. Hamzehpour, and J. Sarabadani, "Electro-osmotic flow in different phosphorus nanochannels," Phys. Fluids **35**, 042006 (2023).

[33]B. Shan, L. Ju, W. Su, Z. Guo, and Y. Zhang, "Non-equilibrium flow of van der Waals fluids in nano-channels," Phys. Fluids **35**, 052004 (2023).

[34]D. Salem, "Collision integrals and viscosity coefficients of argon–carbon thermal plasmas: Comparison using different interaction potentials," Phys. Fluids **34**, 126602 (2022).

[35]M. Buchowiecki, "High-temperature collision integrals for m-6-8 and Hulburt-Hirschfelder potentials," Int. J. Thermophys. **43**, 38 (2022).

[36]M. Klein and H. Hanley, "m-6-8 potential function," J. Chem. Phys. **53**, 4722 (1970).

[37]H. M. Hulburt and J. O. Hirschfelder, "Potential energy functions for diatomic molecules," J. Chem. Phys. **9**, 61 (1941).

[38]J. C. Rainwater, P. M. Holland, and L. Biolsi, "Binary collision dynamics and numerical evaluation of dilute gas transport properties for potentials with multiple extrema," J. Chem. Phys. **77**, 434 (1982).

[39]T.-C. Lim, "Application of extended-Rydberg parameters in general Morse potential functions," J. Math. Chem. **49**, 1086 (2011).

[40]P. Kuntz and A. Roach, "Ion-molecule reactions of the rare gases with hydrogen. Part 1. Diatomics-in-molecules potential energy surface for ArH_2^+," J. Chem. Soc., Faraday Trans. 2 **68**, 259 (1972).

[41]M. Buchowiecki and P. Szabó, "N–H collision integrals with study of repulsive interactions," Plasma Sources Sci. Technol. **31**, 045010 (2022).

[42]F. Sharipov, "Direct simulation Monte Carlo method based on ab initio potential: Recovery of transport coefficients of multi-component mixtures of noble gases," Phys. Fluids **34**, 097114 (2022).

[43]P. Valentini, M. S. Grover, N. Bisek, and A. Verhoff, "Molecular simulation of flows in thermochemical non-equilibrium around a cylinder using *ab initio* potential energy surfaces for $N_2 + N$ and $N_2 + N_2$ interactions," Phys. Fluids **33**, 096108 (2021).

[44]M. S. Grover and P. Valentini, "*Ab initio* simulation of hypersonic flows past a cylinder based on accurate potential energy surfaces," Phys. Fluids **33**, 051704 (2021).

[45]V. Yurkiv, J. Wu, S. Halder, R. Granda, A. Sankaran, A. L. Yarin, and F. Mashayek, "Water interaction with dielectric surface: A combined *ab initio* modeling and experimental study," Phys. Fluids **33**, 042012 (2021).

[46]R. A. Aziz, A. R. Janzen, and M. R. Moldover, "*Ab initio* calculations for helium: A standard for transport property measurements," Phys. Rev. Lett. **74**, 1586 (1995).

[47]M. Buchowiecki, "The elastic scattering cross sections of the N^+–H and N–H^+ collisions for the transport theory," At. Data Nucl. Data Tables **151**, 101574 (2023).

[48]Z. Ding, Z. Qin, and L. Liu, "Collision integrals for $N(^4S)$-$N(^4S)$, $N(^4S)$-$N(^2D)$ and $N(^4S)$-$N(^2P)$ interactions," Phys. Fluids **35**, 027127 (2023).

[49]G. Chen, Z. Qin, J. Li, and L. Liu, "A global CHIPR potential energy surface of PH_2 (X^2B_1) *via* extrapolation to the complete basis set limit and the dynamics of $P(^2D) + H_2$ $(X^1\Sigma^+_g) \rightarrow PH$ $(X^3\Sigma^-) + H(^2S)$," Phys. Chem. Chem. Phys. **24**, 19371 (2022).

[50]X. Li, Z. Qin, J. Li, and L. Liu, "An accurate NH_2 (X^2A'') CHIPR potential energy surface via extrapolation to the complete basis set limit and dynamics of the $N(^2D) + H_2$ $(X^1\Sigma^+_g)$ reaction," Phys. Chem. Chem. Phys. **24**, 26564 (2022).

[51]X. Li, Z. Qin, G. Chen, and L. Liu, "Reaction dynamics of $C(^3P) + Si_2(X^3\Sigma^-_g) \rightarrow Si(^3P) + SiC(X^3\Pi)$ on a global CHIPR potential energy surface of the ground state $Si_2C(X^1A_1)$," Mon. Not. R. Astron. Soc. **522**, 3049 (2023).

[52]G. Chen, Z. Qin, X. Li, and L. Liu, "Reaction dynamics of $P(^4S) + O_2(X^3\Sigma^-) \rightarrow O(^3P) + PO(X^2\Pi)$ on a global CHIPR potential energy surface of $PO_2(X^2A_1)$: Implication for atmospheric modelling," Atmos. Chem. Phys. **23**, 10643–10659 (2023).

[53]A. Varandas, "Combined-hyperbolic-inverse-power-representation of potential energy surfaces: A preliminary assessment for H_3 and HO_2," J. Chem. Phys. **138**, 054120 (2013).

[54]A. Varandas, "Accurate combined-hyperbolic-inverse-power-representation of *ab initio* potential energy surface for the hydroperoxyl radical and dynamics study of O+OH reaction," J. Chem. Phys. **138**, 134117 (2013).

[55]C. M. Rocha and A. J. Varandas, "A general code for fitting global potential energy surfaces via CHIPR method: Direct-fit diatomic and tetratomic molecules," Comput. Phys. Commun. **258**, 107556 (2021).

[56]C. M. Rocha and A. J. Varandas, "A general code for fitting global potential energy surfaces via CHIPR method: Triatomic molecules," Comput. Phys. Commun. **247**, 106913 (2020).

[57]C. Rocha and A. Varandas, "Accurate CHIPR potential energy surface for the lowest triplet state of C_3," J. Phys. Chem. A **123**, 8154 (2019).

[58]Z. Ding, Z. Qin, and L. Liu, "Scattering cross sections and collision integrals for $N(^4S)$–$N^+(^3P)$ and $N(^4S)$–$N^+(^1D)$ interactions," Phys. Fluids **35**, 087120 (2023).

[59]Z. Hou, Z. Qin, and L. Liu, "Transport collision integrals for $C(^5S)$–$H(^2S)$, C (^1S)–$H(^2S)$, $C(^1D)$–$H(^2S)$, and $C(^3P)$–$H(^2S)$ interactions," Phys. Fluids **35**, 087133 (2023).

25 October 2023 11:56:47

[60]H. Werner, P. Knowles, G. Knizia, F. Manby, M. Schütz, P. Celani, W. Györffy, D. Kats, T. Korona, and R. Lindh, see http://www.molpro.net for "MOLPRO, version 2015.1, a package of *ab initio* programs."

[61]H.-J. Werner, P. J. Knowles, F. R. Manby, J. A. Black, K. Doll, A. Heßelmann, D. Kats, A. Köhn, T. Korona, and D. A. Kreplin, "The Molpro quantum chemistry package," J. Chem. Phys. **152**, 144107 (2020).

[62]H. J. Werner and P. J. Knowles, "A second order multiconfiguration SCF procedure with optimum convergence," J. Chem. Phys. **82**, 5053 (1985).

[63]P. J. Knowles and H.-J. Werner, "An efficient second-order MC SCF method for long configuration expansions," Chem. Phys. Lett. **115**, 259 (1985).

[64]H. J. Werner and P. J. Knowles, "An efficient internally contracted multiconfiguration-reference configuration interaction method," J. Chem. Phys. **89**, 5803 (1988).

[65]P. J. Knowles and H.-J. Werner, "An efficient method for the evaluation of coupling coefficients in configuration interaction calculations," Chem. Phys. Lett. **145**, 514 (1988).

[66]P. J. Knowles and H.-J. Werner, "Internally contracted multiconfiguration-reference configuration interaction calculations for excited states," Theor. Chim. Acta **84**, 95 (1992).

[67]K. Shamasundar, G. Knizia, and H.-J. Werner, "A new internally contracted multi-reference configuration interaction method," J. Chem. Phys. **135**, 054101 (2011).

[68]Z. Qin, T. Bai, and L. Liu, "An *ab initio* study for the photodissociation of HCl and HF," Mon. Not. R. Astron. Soc. **516**, 550 (2022).

[69]T. Bai, Z. Qin, and L. Liu, "Radiative association for the formation of MgO," Mon. Not. R. Astron. Soc. **500**, 2496 (2020).

[70]H. Meng, Z. Qin, and L. Liu, "Formation of CO through C ($2s^2 2p^2$ ^{3}P) and O ($2s^2 2p^4$ ^{3}P) radiative association," Astrophys. J. **935**, 148 (2022).

[71]S. Zhang, Z. Qin, and L. Liu, "A quantum mechanical calculation of the CN radiative association," Mon. Not. R. Astron. Soc. **515**, 6066 (2022).

[72]Z. Hou, Z. Qin, and L. Liu, "Formation of SiO$^+$ through radiative association of Si$^+$($3s^2 3p$ ^{2}P$_u$) and O($2s^2 2p^4$ ^{3}P$_g$)," Astron. Astrophys. **672**, A25 (2023).

[73]M. Douglas and N. M. Kroll, "Quantum electrodynamical corrections to the fine structure of helium," Ann. Phys. **82**, 89 (1974).

[74]M. Reiher and A. Wolf, "Exact decoupling of the Dirac Hamiltonian. II. The generalized Douglas–Kroll–Hess transformation up to arbitrary order," J. Chem. Phys. **121**, 10945 (2004).

[75]M. Reiher and A. Wolf, "Exact decoupling of the Dirac Hamiltonian. I. General theory," J. Chem. Phys. **121**, 2037 (2004).

[76]F. Meeks, T. Cleland, K. Hutchinson, and W. Taylor, "On the quantum cross sections in dilute gases," J. Chem. Phys. **100**, 3813 (1994).

[77]S. Matoba, H. Tanuma, and K. Ohtsuki, "Mobility of the metastable C$^+$ ion in cooled He gas at 77 and 4.3 K," J. Phys. B **41**, 145205 (2008).

[78]D. D. Konowalow, J. O. Hirschfelder, and B. Linder, "Low-temperature, low-pressure transport coefficients for gaseous oxygen and sulfur atoms," J. Chem. Phys. **31**, 1575 (1959).

[79]H. Knof, E. Mason, and J. Vanderslice, "Interaction energies, charge exchange cross sections, and diffusion cross sections for N$^+$–N and O$^+$–O collisions," J. Chem. Phys. **40**, 3548 (1964).

[80]M. Capitelli, C. Guidotti, and U. Lamanna, "Potential energy curves and excitation transfer cross sections of excited hydrogen atoms," J. Phys. B **7**, 1683 (1974).

[81]Z. Biglari, A. Shayesteh, and A. Maghari, "Ab initio potential energy curves and transition dipole moments for the low-lying states of CH$^+$," Comput. Theor. Chem. **1047**, 22 (2014).

[82]C. Mbiba Touedebe, C. Nkem, and L. O. Owono, "*Ab initio* calculation of the potential energy curves and spectroscopic properties of low-lying electronic states of CH$^+$ molecular cation," Mol. Phys. **121**, e2151946 (2023).

[83]R. Saxon, K. Kirby, and B. Liu, "Excited states of CH$^+$: Potential curves and transition moments," J. Chem. Phys. **73**, 1873 (1980).

[84]S. Green, P. Bagus, B. Liu, A. D. McLean, and M. Yoshimine, "Calculated potential-energy curves for CH$^+$," Phys. Rev. A **5**, 1614 (1972).

[85]A. W. Kanzler, H. Sun, and K. F. Freed, "Dipole moments, transition moments, oscillator strengths, radiative lifetimes, and overtone intensities for CH and CH$^+$ as computed by quasi-degenerate many-body perturbation theory," Int. J. Quantum Chem. **39**, 269 (1991).

[86]K. Kowalski and P. Piecuch, "The active-space equation-of-motion coupled-cluster methods for excited electronic states: Full EOMCCSDt," J. Chem. Phys. **115**, 643 (2001).

[87]R. Hakalla, R. Kępa, W. Szajna, and M. Zachwieja, "New analysis of the Douglas-Herzberg system (A$^1\Pi$-X$^1\Sigma^+$) in the CH$^+$ ion radical: The A$^1\Pi$-X$^1\Sigma^+$ system in the CH," $^+$Eur. Phys. J. D **38**, 481 (2006).

[88]U. Hechtfischer, C. J. Williams, M. Lange, J. Linkemann, D. Schwalm, R. Wester, A. Wolf, and D. Zajfman, "Photodissociation spectroscopy of stored CH$^+$ ions: Detection, assignment, and close-coupled modeling of near-threshold Feshbach resonances," J. Chem. Phys. **117**, 8754 (2002).

[89]K. P. Huber and G. Herzberg, *Molecular Spectra and Molecular Structure: IV. Constants of Diatomic Molecules* (Van Nostrand, New York, 1979).

[90]U. Hechtfischer, J. Rostas, M. Lange, J. Linkemann, D. Schwalm, R. Wester, A. Wolf, and D. Zajfman, "Photodissociation spectroscopy of stored CH$^+$ and CD$^+$ ions: Analysis of the b $^3\Sigma^-$-a $^3\Pi$ system," J. Chem. Phys. **127**, 204304 (2007).

25 October 2023 11:56:47